DE-FG05-80ET-53088-681 IFSR #681

Analytical and Numerical Studies of Ion Mobility Near the Tokamak Plasma Edge

H. XIAO, R.D. HAZELTINE
Institute for Fusion Studies
The University of Texas at Austin
Austin, Texas 78712
and
P.M. Valanju
Fusion Research Center
The University of Texas at Austin
Austin, Texas 78712

November 1994

Analytical and Numerical Studies of Ion Mobility Near the Tokamak Plasma Edge

H. Xiao, R. D. Hazeltine
Institute for Fusion Studies
The University of Texas at Austin
Austin, Texas 78712
and
P. M. Valanju
Fusion Research Center
The University of Texas at Austin
Austin, Texas 78712

Abstract

The effects of radial electric field on charged particle motion and transport in toroidal magnetic system have been studied both analytically and numerically. The effects of radial electric field on particle orbits are examined, allowing for the relatively large and strongly sheared field observed in some experiments. It is found that ion radial mobility due to the combined effects of radial electric field and charge exchange collisions can dramatically affect the ion transport and orbit loss near the tokamak edge. These properties may help understand the formation of transport barrier near the tokamak plasma edge during high confinement mode (H-mode) discharge and explain the asymmetry between bias voltage and confinement in biased-electrode-induced H-mode.

52.20.Dq, 52.25.Fi

I. INTRODUCTION

In the tokamak edge, plasma transport is especially complex. Edge transport is larger than the neoclassical prediction by factor of 10 to 100. It is widely believed that turbulence due to various instabilities causes this anomalous transport.

Many experimental results have shown that radial electric field has very significant effects on plasma transport and rotation.,[12] It is widely believed that radial electric field plays a very important role in the high confinement mode (H-mode) plasma operation.[3]

There are some theoretical models of the formation of radial electric field near the tokamak plasma edge.[4–6] Also there are many theories about how shear of the radial electric field affects particle movement[4,7,8] and how shear flow (equivalent to radial electric field shear) suppresses turbulence and improves plasma confinement.[9–15]

However, the radial electric field itself deserves more attention, because it can dramatically affect charged particle orbit in toroidal system. The presence of collisions which do not conserve ion momentum leads to ion radial mobility which can significantly affect particle confinement.[17,16]

In 1982, the high confinement mode (H-mode) was discovered in the Axisymmetric Divertor Experiment (ASDEX).[18] It improved the energy confinement time by roughly a factor of two as compared to that obtained in L-mode discharges. Since then, the spontaneous H-mode was observed in many tokamaks with different heating methods, in circular and non circular plasmas and in divertor and limiter configurations.[19–26] It can also be triggered by a biased electrode.[27–30] Spontaneous H-mode has also been observed in Wendelstein-7 Advanced Stellarator (W7-AS),[31] showing that the H-mode is not limited to tokamak geometry. In all these H-mode experiments, transport barriers are observed near the plasma edge. There are many theories about the formation of the transport barrier.[9–15] In this paper, we

propose an alternative explanation based on ion mobility. Many experimental results seem to support our model.

This paper is arranged as follows: in Sec. II, the simulation model and algorithm are discussed. Two kinds of collision operators, pitch angle scattering and charge exchange are developed. Effects of radial electric field on the charged particle guiding-center orbit are discussed in Sec. III. Analytical and numerical studies of neoclassical ion mobility are given in Sec. IV. Relation between ion orbit loss and radial electric field is studied in Sec. V. Discussion and summary are given in Sec. VI.

II. MONTE-CARLO SIMULATION STUDIES

A. Equation of motion

The drift velocity of the ion guiding center in a toroidal system at low plasma pressure can be written as:

$$\mathbf{v}_d = v_{||}\frac{\mathbf{B}}{B} + \frac{1}{\Omega}\left(v_{||}^2 + \frac{v_\perp^2}{2}\right)\frac{\mathbf{B}\times\nabla B}{B^2} + \frac{c\mathbf{E}\times\mathbf{B}}{B^2}. \tag{1}$$

Here $v_{||} = \mathbf{v}\cdot\mathbf{B}/B$ is the guiding center velocity parallel to the magnetic field and $v_\perp$ is the guiding center velocity perpendicular to the magnetic field. The equation of motion of the ion guiding center can be written as

$$\frac{d\mathbf{x}}{dt} = \mathbf{v}_d. \tag{2}$$

We approximate the tokamak magnetic field by $\mathbf{B} = B_0(1 - x/R)\widehat{z} + B_\theta\widehat{\theta}$, where R is the major radius of tokamak, B_0 is the magnetic field on toroidal axis, B_θ is the poloidal magnetic field due to the plasma toroidal current, $B_\theta \ll B_0$. We also assume that $\mathbf{E} = E_r\widehat{r}$. Here $\widehat{r} = (x\widehat{\mathbf{x}} + y\widehat{\mathbf{y}})/r$ is the unit radial vector, $\widehat{\theta} = (-y\widehat{\mathbf{x}} + x\widehat{\mathbf{y}})/r$ is the unit vector in poloidal direction and $\widehat{z} = R\nabla\zeta$ is the unit vector in toroidal direction.

The components of Eq. (2) take the form

$$\frac{dx}{dt} = -\left(\frac{v_\parallel}{qR} - \frac{cE_r}{Br}\right) y, \tag{3}$$

$$\frac{dy}{dt} = \left(\frac{v_\parallel}{qR} - \frac{cE_r}{Br}\right) x - \frac{1}{\Omega R}\left(v_\parallel^2 + \frac{v_\perp^2}{2}\right), \tag{4}$$

$$\frac{dz}{dt} = v_\parallel + \frac{1}{\Omega R^2 q}\left(v_\parallel^2 + \frac{v_\perp^2}{2}\right)\left(\frac{B_0}{B}\right)^2 x + \frac{E_r}{qB}\frac{r}{R} \tag{5}$$

where x, y and z are ion positions in the Cartesian coordinate system with the origin at the magnetic axis of the tokamak, $r = \sqrt{x^2 + y^2}$, and q is the safety factor, modeled by $q(r) = q_a(1 + r^2)^2/4$ ($q_a = 4$ is chosen for the simulations in this paper). We can solve these equations by 4th order Runge-Kutta integration.[32]

B. Pitch angle scattering

In this work, we use Berk and Ye's[35] modified pitch-angle scattering operator:

$$\Delta\xi = -\nu_c\tau\xi + \sigma\sqrt{\nu_c\tau(1 - \xi^2 + \nu_c\tau)}. \tag{6}$$

where $\Delta\xi$ is a small change of pitch angle in a small time interval (τ) as shown in Fig. 1. To simulate the small angle scattering, σ is randomly assigned the value of ± 1 for each τ. Notice that Eq. (6) is slightly different from Boozer and Kuo-Petravic's pitch-angle scattering operator.[34] An additional term $\nu_c\tau$ is introduced in the square root next to $1 - \xi^2$. This makes it possible to simulate the pitch angle at $\xi = 1$, where a "dead end" would otherwise arise.

C. Charge-exchange

When an ion collides with a neutral particle, there is a chance that the ion and neutral may exchange roles via charge exchange (CX). We can easily simulate the CX process numerically by using its physical characteristics. At every step of the ion orbit, we give it a chance to

collide with the neutral. If it takes that chance, as at the second and the third points of Fig. 2, we determine that CX happened. Then we reload the ion at the same spatial place, while its velocity is changed according to the neutral distribution. This procedure gives a natural way to simulate the CX process.

D. Test of the code

We can test the code by comparing the pitch-angle scattering results with neoclassical theory of electron transport. The standard diagnostic procedure is designed for calculating the random walk diffusion coefficient D of the Brownian particles.[36] The time-dependent diffusion coefficient is defined by

$$D(t) = \lim_{t\to\infty} \frac{1}{2Nt} \sum_{i=1}^{N} [r_i(t) - r_i(0)]^2, \tag{7}$$

where $r_i(t)$ is the radial position of the ith particle at time t, and $N = 1000$ is the total number of particles for the simulation. One thousand particles with Maxwellian velocity distribution are pre-loaded at $r/a = 0.5$, where $q = 1.56$, and $r/R = 0.1$. Other parameters are: $\rho/a = 0.002$ and $\nu/(v_t/R) = 0.005$. From Fig. 3 we see that the time-dependent diffusion coefficient $D(t)$ saturates in less than 10 t_0 time units, ($t_0 = R/v_t$). From the slope of the Δr^2 curve we can find that the diffusion coefficient is about 5×10^{-7}, which agrees well with the neoclassical value[37,38] $D \approx \nu\rho^2 q^2/\epsilon^{3/2} \approx 9.8 \times 10^{-7}$.

The saturated D versus ν_c is shown in Fig. 4 by the dotted curve

$$D_{\text{banana}} = \nu_{ii}\rho_i^2 q^2 \epsilon^{-3/2};$$

line (b) is the theoretical value in plateau regime,

$$D_{\text{plateau}} = \frac{v_t}{Rq}\rho_i^2 q^2;$$

and line (c) is the theoretical value in Pfirsch-Schlüter regime,

$$D_{\text{PS}} = \nu_{ii}\rho_i^2 q^2.$$

Here $\nu_{ii} = \nu_c/2$ has been adopted for the quoted expressions. One property of neoclassical theory is the correlation between the transport coefficients and collision frequency. This feature is indeed reproduced by the present Monte-Carlo simulation, as shown in Fig. 4.

III. PARTICLE ORBITS IN TOROIDAL SYSTEM

We can get the neoclassical orbits of charged particles in an axisymmetric system by using the drift conservation laws. They are the conservation of particle energy,

$$H = \frac{1}{2} m v^2 + e\phi = \frac{1}{2} m v_0^2 + e\phi_0, \tag{8}$$

magnetic momentum

$$\mu = \frac{v_\perp^2}{2B} = \frac{v_{\perp 0}^2}{2B_0}, \tag{9}$$

and toroidal angular moment,

$$p_\zeta = mRv_{||} - \frac{e}{c}\chi = mR_0 v_{||0} - \frac{e}{c}\chi_0. \tag{10}$$

Where the subscripts $_0$ indicate the starting point of the charged particle orbit.

From Eqs. (8) and (9), we can get

$$v_{||} = v_0 \sqrt{1 - \frac{B}{B_0}(1 - \xi_0^2) - \frac{e(\phi - \phi_0)}{w_0}}, \tag{11}$$

where $v_0 = \sqrt{v_{\perp 0}^2 + v_{||0}^2}$, $w_0 = \frac{1}{2} m v_0^2$ and $\xi_0 = v_{||0}/v_0$. From Eq. (10) and using

$$\chi - \chi_0 \approx R_0 B_p (r - r_0),$$

we have

$$v_{||} \approx v_0 \frac{R_0}{R} (\xi_0 + X), \tag{12}$$

where $X = (r - r_0)/\rho_p$ is normalized orbit width, $\rho_p = v_0/(eB_p/mc)$ is the gyroradius of the charged particle at the starting point. From Eqs. (11) and (12) we can get the particle trajectory equation

$$(\xi_0 + X)^2 + (1 - \xi_0^2) Y - \left(1 - \frac{e(\phi - \phi_0)}{w_0}\right) Y^2 = 0 \tag{13}$$

where $Y = B_0/B \approx R/R_0$. Introducing $\Delta = |Y - 1|$ and note that $\Delta = (R - R_0)/R_0 \leq r/R_0 = 2\epsilon \ll 1$, we can get

$$\Delta \approx \frac{X^2 + 2\xi_0 X + e(\phi - \phi_0)/w_0}{1 + \xi_0^2 - 2e(\phi - \phi_0)/w_0}. \tag{14}$$

From Fig. 5 we find that the trajectory size can be determined from the two conditions:

$$\Delta = \pm\frac{2r_0 + \Delta r}{R_0} \approx \pm 2\epsilon \qquad \text{for passing particles}$$

and

$$\Delta = \pm\frac{\Delta r}{R_0} \approx 0 \qquad \text{for trapped particles.}$$

We concentrate our attention on the effects of the constant radial electric field on charged particle motion in the toroidal system. Thus the electric potential in Eq. (14) can be expanded as

$$\phi - \phi_0 \approx -E_r(r - r_0). \tag{15}$$

We can obtain the particle orbit width from these two equations:

$$X^2 + 2\xi_0 X - 2\overline{V}_{Ep} X \approx 0 \tag{16}$$

for trapped particles and

$$X^2 + 2\xi_0 X - 2\overline{V}_{Ep} X + 2\epsilon(1 + \xi^2 + 4\overline{V}_{Ep} X) \approx 0 \tag{17}$$

for passing particles, where $\overline{V}_{Ep} = cE_r/v_0 B_p$ is the normalized radial electric field. The orbit size with constant radial electric field in toroidal geometry can be expressed as:

$$X = \min\left\{2(\overline{V}_{Ep} - \xi_0), \quad \overline{V}_{Ep}(1 - 4\epsilon) - \xi_0 - \sqrt{(\overline{V}_{Ep}(1 - 4\epsilon) - \xi_0)^2 - 2\epsilon(1 + \xi_0^2)}\right\}. \tag{18}$$

The first term on right-hand side of Eq. (18) is the orbit width of trapped particles and the second term is the orbit width of passing particles. When

$$(\overline{V}_{Ep}(1 - 4\epsilon) - \xi_0)^2 - 2\epsilon(1 + \xi^2) < 0, \tag{19}$$

there are no solutions for passing particle orbit width, therefore the particle must be in trapped orbit.

When radial electric field becomes very large, $|\overline{V}_{Ep}| \gg 1$, the trapping condition of Eq. (19) is no longer satisfied, therefore all particles are in passing orbits with orbit widths:

$$X \approx \frac{\epsilon(1+\xi_0^2)}{\overline{V}_{Ep}(1-4\epsilon)-\xi_0}.$$

It will tend to zero proportional to the $\overline{V}_{Ep}^{-1}$.

In toroidal geometry, the radial electric field combine with collision can affect ion orbits dramatically.[16] With collisions we find that without radial electric field the particle motion is just random diffusion, as shown in Fig. 6. With positive radial electric field, the ion drift motion tends to move them outward as shown in Fig. 7; with negative radial electric field ions drift motion tends to move them inward as shown in Fig. 8.

Putting N particles with Maxwellian velocity distribution in the toroidal system, we can calculate the average orbit shift by running the Monte Carlo simulation code without collisions and taking the average on both time and particles:

$$\langle \Delta r \rangle = \frac{1}{N}\frac{1}{J}\sum_i^N \sum_j^J (r_i(\Delta t * j) - r_0).$$

Where Δt is the calculation time step, J is the total number of time steps for each particle ($\Delta t * J \gg R/v_t$), and $N = 1000$ is the particle numbers. The average orbit shift change with radial electric field is shown in Fig. 9. We can understand these orbits from the previous discussion.[39,40]

The positive radial electric field pushes the particles outward where the total magnetic field is weaker, hence the orbit width is larger. For the same reason the orbit width corresponding to the negative radial electric field is smaller. This helps us understand the small asymmetry of the effect of radial electric field on both orbit width and random walk distance. It is also helpful in understanding the asymmetric effect of radial electric field on ion radial mobility and diffusion.

Without radial electric field, the average orbit width for the Maxwellian particles should be zero, because the positive orbit shift and the negative orbit shift would cancel each other leaving no net orbit shift. With radial electric field, the orbit shifts are no longer in balance: there is a net average orbit shift. When radial electric field becomes strong, many of the particles will be pushed into passing orbits and the net orbit shift will be reduced. When radial electric field gets very strong, almost all particles land in the passing orbit which stay very close to their original flux surface, leading to almost no net orbit shift.

We can also get the random walk distance at the same time by calculating:

$$\left\langle \Delta r^2 \right\rangle = \frac{1}{N}\frac{1}{J}\sum_{i}^{N}\sum_{j}^{J}\left(r_i(\Delta t * j) - r_0\right)^2 .$$

The results are shown in Fig. 10. We find that the neoclassical particle diffusion coefficient is:

$$D \approx \nu \left\langle \Delta r^2 \right\rangle$$

and for momentum non-conserving collisions, the ion mobility is:

$$\langle V_r \rangle \approx \nu \langle \Delta r \rangle$$

IV. NEOCLASSICAL ION MOBILITY

In many theoretical works, the effect of radial electric field shear on the particle orbits[4,5,7,8] and on suppressing turbulence,[9–11] have been studied. However we find that the radial electric field itself can significantly affect particle radial transport; hence it also deserves attention.[16,17]

In the plasma edge, the plasma temperature and density are much lower than in the core region and the neutral concentration is much higher. Therefore collisions between ions and neutrals could be important there. These charge exchange collisions are momentum non-conserving. Thus ambipolarity could be broken in plasma edge. In this case, since the

radial electric field affects the particle step size it can cause a dramatic change of particle flux.

A. Neoclassical mobility in the banana regime

In banana regime the collisions are very weak, and it is difficult to get the neoclassical mobility from drift kinetic equation. Hence we use the single particle approach here.[41] For large aspect ratio $\epsilon \ll 1$, the r and θ components of the single particle drift velocity in tokamak geometry can be written as:

$$\frac{dr}{dt} = -\frac{1}{\Omega R}\left(v_{||}^2 + \frac{v_\perp^2}{2}\right)\sin\theta, \tag{20}$$

$$r\frac{d\theta}{dt} = \Theta v_{||} - \frac{1}{\Omega R}\left(v_{||}^2 + \frac{v_\perp^2}{2}\right)\cos\theta - \frac{cE_r}{B}, \tag{21}$$

where $\Theta = B_\theta/B$. The toroidal angular momentum is:

$$p_\zeta = mRv_{||} - \frac{e}{c}\chi. \tag{22}$$

With collisions, p_ζ is no longer a constant of motion. However, its change is very small with weak collisions, we can still treat it as an invariance. Therefore we have

$$\frac{dp_\zeta}{dt} = mv_{||}\frac{dR}{dt} + mR\frac{dv_{||}}{dt} - \frac{e}{c}\chi'\frac{dr}{dt} \approx 0. \tag{23}$$

$$\frac{dv_{||}}{dt} + \frac{v_{||}}{R}\frac{d}{dt}(r\cos\theta) - \Omega_p\frac{dr}{dt} = 0, \tag{24}$$

By substituting Eqs. (20) and (21) into Eq. (24) and using

$$\frac{\delta v_{||}}{\delta t} = -\nu_c v_{||},$$

where $\delta v_{||}$ is the parallel velocity change due to collisions, we can obtain:

$$\nu_c\left\langle v_{||}\right\rangle = -\frac{r}{qR^2}\left(\frac{v_\perp^2}{2}\left\langle\sin\theta\right\rangle + V_{Ep}\left\langle v_{||}\sin\theta\right\rangle\right). \tag{25}$$

Where $V_{Ep} = cE_r/B_p$. Assuming $\left\langle v_{||} \sin\theta \right\rangle \approx \left\langle v_{||} \right\rangle \langle \sin\theta \rangle + \cdots$ and $\left\langle v_{||} \right\rangle \approx V_{Ep}$,[42] we get:

$$\langle \sin\theta \rangle = -\frac{\nu_c V_{Ep}}{\frac{r}{qR^2}\left(\frac{v_\perp^2}{2} + V_{Ep}^2\right)}. \tag{26}$$

From Eqs. (20) and (26) we can get:

$$\left\langle \frac{dr}{dt} \right\rangle = \frac{\nu_c}{\Omega_p}\left(\frac{v_\perp^2}{2} + v_{||}^2\right)\frac{V_{Ep}}{\frac{v_\perp^2}{2} + V_{Ep}^2}. \tag{27}$$

The physics behind the derivation of the V_{Ep}^2 term in the denominator of Eq. (27) lies in the off-diagonal viscosity, the second term of Eq. (24). We can get the plasma mobility by integrating the single particle radial velocity of Eq. (27) over the Maxwellian distribution

$$\langle V_r \rangle = \int \left\langle \frac{dr}{dt} \right\rangle f_M d\mathbf{v}.$$

After some simple manipulations we can get:

$$\langle V_r \rangle = \frac{\nu_c}{\Omega_p} v_t \tilde{V}_{Ep}\left[1 - \left(1 - 2\tilde{V}_{Ep}^2\right)\exp\left(-2\tilde{V}_{Ep}^2\right)\mathrm{Ei}\left(-2\tilde{V}_{Ep}^2\right)\right], \tag{28}$$

where

$$\mathrm{Ei}(x) = -\int_{-x}^{\infty} \frac{e^{-t}}{t} dt$$

is the second exponential integral function.

B. Neoclassical mobility in plateau regime

In plateau regime we try to get the neoclassical mobility from the drift kinetic equation, which can be written as[43]:

$$\frac{\partial f}{\partial t} + \{H, f\} = \left(\frac{\partial f}{\partial t}\right)_{\mathrm{coll}}, \tag{29}$$

where

$$\{H, f\} \equiv \left\{-\frac{1}{\Omega R}\left(v_{||}^2 + \frac{v_\perp^2}{2}\right)\sin\theta\frac{\partial}{\partial r} + \left[-\frac{1}{\Omega R}\left(v_{||}^2 + \frac{v_\perp^2}{2}\right)\cos\theta + \right.\right.$$

$$\left.\left.\Theta v_{||} - \frac{cE_r}{B}\right]\frac{\partial}{\partial\theta} - \frac{\Theta}{R}\left(v_{||}^2 + \frac{v_\perp^2}{2}\right)\sin\theta\frac{\partial}{\partial v_{||}}\right\} f$$

and $(\frac{\partial f}{\partial t})_{\text{coll}}$ is the collision operator. For charge exchange collisions, we use the first order Krook expression[44]:

$$\left(\frac{\partial f}{\partial t}\right)_{\text{coll}} \approx \nu\,(f - f_0) = -\nu f^{(1)}$$

For the plateau regime, collisions are frequent enough to establish a Maxwellian distribution. The limitation on the collision frequency can be expressed by the inequality:

$$\epsilon^{3/2}\frac{v_t}{qR} < \nu < \frac{v_t}{qR}. \tag{30}$$

The solution of the kinetic equation can be sought in the form of an expansion in the toroidal parameter. We write the distribution function in the form:

$$f(v_\perp, v_{||}, r, \theta) = f^{(0)}\left(v_\perp, v_{||}, r\right) + f^{(1)}(v_\perp, v_{||}, r, \theta\Big) \tag{31}$$

where

$$f^{(0)} = \frac{n_0(r)}{\pi^{3/2}v_t^3}\exp\left[\frac{v_\perp^2 + v_{||}^2}{v_t^2} - \frac{2e\Phi(r)}{v_t^2}\right]$$

is a local Maxwellian function while the correction $f^{(1)}$ takes account of toroidal effects. We can linearize Eq. (29) to obtain:

$$(\Theta v_{||} - V_E)\frac{\partial f^{(1)}}{r\partial\theta} = -\nu f^{(1)} + \frac{1}{R}\left(v_{||}^2 + \frac{v_\perp^2}{2}\right)\sin\theta\left[\Theta\frac{\partial}{\partial v_{||}} + \frac{1}{\Omega}\frac{\partial}{\partial r}\right]f^{(0)}. \tag{32}$$

We can solve this equation and get the following form:

$$f^{(1)} = \frac{\nu\sin\theta}{R}\left(v_{||}^2 + \frac{v_\perp}{2}\right)\left(\Theta\frac{\partial}{\partial v_{||}} - \frac{1}{\Omega}\frac{\partial}{\partial r}\right)f^{(0)} \Big/ \left[\left(\Theta\frac{v_{||}}{r} - \frac{V_E}{r}\right)^2 + \nu^2\right]. \tag{33}$$

Multiplying this expression by the radial drift velocity and integrating over velocity, we can get the particle flux across the magnetic surface:

$$\langle nV_r\rangle = \int_0^{2\pi} d\theta \int_0^\infty v_\perp dv_\perp \int_{-\infty}^\infty dv_{||} f^{(1)}\frac{dr}{dt}. \tag{34}$$

Substituting Eqs. (20) and (33) into Eq. (34), and using the approximation:

$$\lim_{a\to 0}\frac{a}{x^2 + a^2} \approx \pi\delta(x)$$

we can get the particle flux for the plateau regime:

$$\langle nV_r \rangle = \pi^{1/2} \frac{n(r)\epsilon^2 \rho v_t}{4r} \left(2\tilde{V}_{Ep} - \frac{\rho_p}{n} \frac{\partial n}{\partial r} \right) \left(1 + 2\tilde{V}_{Ep}^2 + 2\tilde{V}_{Ep}^4 \right) \exp\left(-\tilde{V}_{Ep}^2 \right). \tag{35}$$

From Eq. (35), we find that the cross field flux in the plateau regime contains two parts. One is the diffusion term, which can be expressed as:

$$D = \frac{\pi^{1/2} \epsilon^2 \rho^2 v_t}{4r\Theta} \left(1 + 2\tilde{V}_{Ep}^2 + 2\tilde{V}_{Ep}^4 \right) \exp\left(-\tilde{V}_{Ep}^2 \right). \tag{36}$$

Another one is the neoclassical mobility:

$$\langle V_r \rangle = \pi^{1/2} \epsilon^2 \frac{\rho}{2r} v_t \tilde{V}_{Ep} \left(1 + 2\tilde{V}_{Ep}^2 + 2\tilde{V}_{Ep}^4 \right) \exp\left(-\tilde{V}_{Ep}^2 \right). \tag{37}$$

Without radial electric field, $\tilde{V}_{Ep} = 0$, we find that the diffusion coefficient becomes:

$$D = \pi^{1/2} \frac{v_t}{4R} \rho^2 q$$

which is consistent with neoclassical theories.[37,43]

C. Simulation results of neoclassical mobility

The Monte Carlo simulation results of the ion mobility change with pitch-angle scattering in the banana regime are shown in Fig. 11. The parameters of the simulation are: $\nu/(v_t/R) = 0.005$, $a/R = 0.2$, $\rho/a = 0.002$, and $q_a = 4$. To avoid prompt particle orbit loss, we put $N = 1000$ particles at $r_0/a = 0.5$ in the beginning. The theoretical curve is calculated from Eq. (280 by using *Mathematica*™.[45] We find that the simulation results match the analytical results fairly well.

Because the orbit is an intrinsic property of the ion motion, we expect that different collision processes will not change the basic property of the ion mobility, thus we should get similar results with charge exchange collision. Using the same parameters as Fig. 11, the Monte-Carlo simulation results with charge exchange collision operator shown in Fig. 12 support our expectation.

In plateau regime, results of ion mobility and diffusion coefficient from Monte Carlo simulation are shown in Figs. 13 and 14, respectively. The charge exchange collision frequency in the simulation is $\nu/(v_t/R) = 0.05$, other parameters are the same as those in Fig. 11. The theoretical curves are calculated from Eqs. (36) and (37). We find that the simulation results agree very well with the theoretical expectation.

V. ION ORBIT LOSS

We put 1000 ions near the plasma edge, $r_0/a = 0.925$, in order to study how the radial electric field affects the ion orbit loss. The Monte-Carlo simulation results of the ion orbit loss in banana regime ($\nu/(v_t/R) = 0.005$) and plateau regime ($\nu/(v_t/R = 0.05$) with charge exchange collision operator under different radial electric fields are shown in Figs. 15 and 16, respectively.

Simulations with pitch angle scattering collision operator give similar results. We find that without radial electric field the ion orbit loss is mainly due to neoclassical diffusion caused by collisions, charge exchange or pitch angle scattering. When the radial electric field is negative, the inward ion mobility reduces the ion orbit loss significantly, and quickly stops the ion loss when radial electric field increases negatively.

When the electric field is positive, ion orbit loss increases very fast at first, due to the positive ion radial mobility. When radial electric field further increases, many ions become passing particles which dramatically reduces the ion loss. When the radial electric field becomes very large, almost all ions are detrapped and compressed close to their original flux surface. That eventually stops the ion orbit loss.

From the simulation we find that it is relatively easy to form the transport barrier with negative radial electric field, because the negative radial mobility can quickly stop the ion orbit loss. Obviously it is harder to form the transport barrier with positive radial electric

r_s	0.875	0.90	0.925	0.95	0.975
$N_{\text{loss}}(L_-)$	137	109	60	37	84
$N_{\text{loss}}(L_+)$	254	318	358	218	63
$N_{\text{loss}}(H_-)$	57	245	229	358	112
$N_{\text{loss}}(H_+)$	229	198	123	49	27
$N_{\text{loss}}(H_{-2})$	233	297	326	966	197
$N_{\text{loss}}(H_{+2})$	216	142	58	22	12

Table 1: Ion orbit loss with different radial sheared radial electric fields in banana regime

r_s	0.875	0.90	0.925	0.95	0.975
$E_r(L_+)$	9.52	16.16	0.	-16.16	-9.52
$E_r(H_+)$	-3.51	-8.65	-12.5	-8.65	-3.51

Table 2: Radial electric fields at r_0.

field because it needs a very strong positive radial electric field to detrap and compress the ion orbit, and stop ion orbit loss.

To investigate how electric field shear affects ion orbit loss, we have chosen two kinds of electric potentials for the simulation. The results of their effects on ion orbit loss are shown in Table 1. Without radial electric field, the ion orbit loss is $N_{\text{loss}} = 213$. The results show that negative radial electric field always improves particle confinement. Simulation parameters are: $\Delta r = 0.04$, $r_0/a = 0.925$, $\nu/(v_t/R) = 0.005$, $a/R = 0.2$, $\rho/a = 0.002$, and $q_a = 4$.

In Table 1, H represents the hyperbolic tangent form of radial electric potential:

$$\phi(r) = \frac{\phi_0}{2}\left[\tanh\left(\frac{r - r_s}{\Delta r}\right) + 1\right]$$

$H_\pm$ means $e\phi_0/mv_t^2 = \pm 1$ and $H_{\pm 2}$ means $e\phi_0/mv_t^2 = \pm 2$. L represents the Lorentz form of radial electric potential:

$$\phi(r) = \phi_0 \Big/ \left[1 + \left(\frac{r - r_s}{\Delta r}\right)^2\right]$$

$L_\pm$ means $e\phi_0/mv_t^2 = \pm 1$. The radial electric fields at r_0 with different r_s for L_+ and H_+ type electrostatic potentials are listed in Table 2.

VI. DISCUSSION AND SUMMARY

In plasma center, there are almost no neutrals at all due to the high plasma temperature and high plasma density, thus ions only collide with electrons or other ions. Because Coulomb collisions conserve momentum, there is no ion radial mobility in the tokamak plasma center region. Ion radial mobility is only important near the plasma edge where charge exchange collisions are abundant.

We can use the of ion radial mobility to understand the transport barrier near the spontaneous H-mode plasma edge. Note that for the spontaneous H-mode plasma there is always a negative electric field near the edge. Thus the inward ion mobility may sharply slow down the outward ion flow, and cause the transport barrier.

The asymmetry of the bias potential and plasma confinement observed in the experiments can be understood by the different mechanisms of forming a transport barrier due to the negative and positive radial electric fields. For the positive bias, which causes a negative radial electric field in the plasma edge, the transport barrier is due to the negative radial mobility, so that it is relatively easy to achieve H-mode. For the negative bias, which causes a positive electric field, it requires a very strong bias potential to achieve strong electric field that could detrap and compress passing particle orbit and form the transport barrier and achieve H-mode.

From TEXT-U experiment results,[46] the edge plasma parameters are: $E_r \approx 40\,\mathrm{V/cm}$, $T_e \approx T_i \approx 30\,\mathrm{eV}$, $n_e \approx 2^{12}\ \mathrm{cm}^{-3}$, and $\partial n_e/\partial r \approx 1 \times 10^{12}\ \mathrm{cm}^{-4}$. The outward particle flux due the turbulence, poloidal asymmetry of electrostatic potential,[47] neoclassical transport and ion radial mobility are listed in the following.

$$\Gamma^{\text{turbulence}} \approx 1.5 \times 10^{20}\mathrm{m}^{-2} \cdot \mathrm{s}^{-1}$$

$$\Gamma^{\text{convection}}_{\text{max}} \approx 0.74 \times 10^{20}\mathrm{m}^{-2} \cdot \mathrm{s}^{-1}$$

$$\Gamma^{\text{neoclassic}} \approx 2.0 \times 10^{17} \text{m}^{-2} \cdot \text{s}^{-1}$$

$$\Gamma^{\text{mobility}} \approx 0.4 \times 10^{20} \text{m}^{-2} \cdot \text{s}^{-1}$$

Where $\Gamma^{\text{turbulence}}$ and $\Gamma^{\text{convection}}_{\text{max}}$ are from Ref. 46, while $\Gamma^{\text{neoclassical}}$ and Γ^{mobility} are calculated from Eqs. (36) and (37), respectively. We find that the particle flux caused by ion radial mobility is of the same magnitude as that caused by turbulence in the plateau regime.

There is no doubt that turbulence suppression by shear flow (sheared radial electric field) plays a very important role in the formation of transport barrier near the H-mode plasma edge. However the ion mobility and electrostatic detrapping and orbit width compression due to radial electric field itself could also be a strong alternative for the formation of transport barrier in H-mode plasma edge.

In summary, neoclassical ion radial mobility due to the combined effects of radial electric field and collision with background particles is found both numerically and analytically. It may provide an alternative approach to understanding the spontaneous H-mode and biased electrode triggered H-mode.

Acknowledgment

We acknowledge the helpful discussion with Dr. P. Yushmanov, Dr. H. C. Ye and Dr. Y. Z. Zhang. Author H. Xiao thanks for the helpful discussions with Dr. J. Q. Dong. This work was supported by the U.S. Department of Energy contract #DE-FG05-80ET-53088.

REFERENCES

[1]K. H. Burrell, E. J. Doyle, P. Gohil, R. J. Groebner, J. Kim, R. J. La Haye, L. L. Lao, R. A. Moyer, T. H. Osborne, W. A. Peebles, C. L. Rettig, T. H. Rhodes, and D. M. Thomas, Phys. Plasmas **1**, 1536 (1994).

[2]N. Asakura, R. J. Fonck, K. P. Jaehnig, S. M. Kaye, B. LeBlanc, and M. Okabayashi, Nucl. Fusion **33**, 1165 (1994).

[3]R. J. Groebner, Phys. Fluids B **5**, 2343, 1993.

[4]R.D. Hazeltine, Phys. Fluids B **1**, 2031 (1989).

[5]H. Xiao, R. Carrera, and R. D. Hazeltine, Nucl. Fusion **31**, 2162 (1991).

[6]R. D. Hazeltine, H. Xiao, and P. M. Valanju, Phys. Fluids B **5**, 4011 (1993).

[7]K. C. Shaing, Phys. Fluids B **4**, 290 (1992).

[8]Y.-Q. Tao, R.W. Conn, L. Schmitz, and G. Tynan, Phys. Fluids **5**, 344 (1993).

[9]H. Biglari, P.H. Diamond, and P.W. Terry, Phys. Fluids B **2**, 1 (1990).

[10]K. R. Shaing, E. C. Crume, Jr., and W. A. Houlberg, Phys. Fluids B **2**, 1492 (1990).

[11]Y. Z. Zhang and S. M. Mahajan, Phys. Fluids B **4**, 1385 (1992)

[12]S. Hamaguchi and W. Horton, Phys. Fluids B **4**, 319 (1992)

[13]J. Q. Dong and W. Horton, Phys. Fluids B **5** 1851, 1993.

[14]J. F. Drake, T. M. Antonsen, J. M. Finn, P. N. Guzdar, A. B. Hassam, C. S. Liu, D. McCarthy, F. W. Waelbroeck, G. G. Craddock, P. H. Diamond, Y. B. Kim, A. W. Hyatt,

T. H. Jensen, A. W. Leonard, H. Biglari, C. K. Philips, and M. Ono, *Plasma Physics and Controlled Nuclear Fusion Research*, Vol. 2, Würzburg, Germany, 1992 (International Atomic Energy Agency, Vienna, 1993), p. 115.

[15]N. Mattor and P. H. Diamond, Phys. Rev. Lett. **72**, 486 (1994).

[16]H. Xiao, R.D. Hazeltine, Y.Z. Zhang, and P.M. Valanju, Phys. Fluids B **5**, 4499 (1993).

[17]H. Xiao, R.D. Hazeltine, P.M. Valanju, and Y.Z. Zhang, *Monte-Carlo Simulation Studies of Effects of Electric Field on Particle Motion in the Tokamak Plasma*, Bull. Am. Phys. Soc. **38**, 1928 (1993).

[18]F. Wagner, G. Becker, K. Behringer, D. Campbell, A. Eberhangen, W. Engelhardt, G. Fussmann, O. Gehre, J. Gernhardt, G. v. Gierke, G. Hass, M. Huang, F. Karger, M. Keilhacker, O. Kluber, M. Kornherr, K. Lackner, G. Lisitano, G. G. Lister, H. M. Mayer, D. Meisel, E.R. Muller, H. Murmann, H. NIedermeyer, W. Poschenrieder, H. Rapp, H. Rohr, F. Schneider, G. Siller, E. Speth, A. Stabler, K. H. Steuer, G. Venus, and O. Vollmer, Phys. Rev. Lett. **49**, 1408 (1982).

[19]S. M. Kaye, M. G. Bell, K. Bol, D. Boyd, K. Brau, D. Buchenauer, R. Budny, A. Cavallo, P. Couture, T. Crowley, D. S. Darrow, H. Eubank, R. J. Fonck, R. Goldston, B. Grek, K. P. Jaehnig, D. Johnson, R. Kaita, H. Kugel, B. LeBlanc, J. Manickam, D. Manos, D. Mansfield, E. Mazzucato, R. McCann, K. McGuire, D. Mueller, A. Murdock, M. Okabayashi, K. Okano, D. K. Owens, D. E. Post, M. Reusch, G. L. Schmidt, S. Sesnic, R. Slusher, S. Suckewer, C. Surko, H. Takahashi, F. Tenney, H. Towner, and J. Valley, J. Nucl. Mater. **121**, 115 (1984).

[20]A. Tanga, K. H. Behringer, A. E. Costley, M. Brusati, B. Denne, A. Edwards, A. Gibson, R. D. Gill, N. Gottardi, R. Granetz, P. J. Harbour, H. Jackel, M. Keihacker, E. Lazzaro,

M. Malacarne, P. D. Morgan, P. Noll, J. Orourke, P. E. Stott, D. R. Summers, J. A. Tagle, and P. R. Thomas, Nucl. Fusion **27**, 1877 (1987).

[21]T. H. Osborne, N. H. Brooks, K. H. Burrell, T. N. Carlstrom, R. J. Groebner, W. Howl, A. G. Kellman, L. L. Lao, T. S. Taylor, D. N. Hill, N. Ohyabu, and M. E. Perry, Nucl. Fusion **30**, 2023 (1990).

[22]S. Sengoku, A. Finahashi, M. Hasegawa, K. Hoshino, S. Kasai, T. Kawakami, H. Kawashima, T. Matoba, T. Matsuda, H. Matsumoto, Y. Miura, M. Mori, H. Ogawa, T. Ohtsuka, T. Shoji, N. Suzuki, H. Tamai, Y. Uesugi, T. Yamamoto, and T. Yamaguchi, Phys. Rev. Lett. **59**, 450 (1987).

[23]S. M. Kaye, J. Manickam, N. Asakura, R. E. Bell, Y.-T. Lau, B. LeBlanc, C. E. Kessel, H. W. Kugel, S. F. Paul, and H. Takahashi, Nucl. Fusion **30**, 2621 (1990).

[24]H. Ninomiya and the JT-60 team, Phys. Fluids B **4**, 424 (1992).

[25]K. Toi, J. Gernhardt, O. Klueber, and M. Kornherr, Phys. Rev. Lett. **62**, 430 (1990).

[26]C. E. Bush, R. J. Goldston, S. D. Scott, E. D. Fredrickson, K. McGuire, J. Schivell, G. Taylor, C. W. Barnes, M. G. Bell, R. L. Boivin, N. Bretz, R. V. Budny, A. Cavallo, P. C. Efthimion, B. Grek, R. Hawryluk, K. Hill, R. A. Hulse, A. Janos, D. W. Johnson, S. Kilpatrick, D. M. Manos, D. K. Mansfield, D. M. Meade, H. Park, A. T. Ramsey, B. Stratton, E. J. Synakowski, H. H. Towner, R. M. Wieland, M. C. Zarnstorff, and S. Zweben, Phys. Rev. Lett. **65**, 424 (1990).

[27]R. J. Taylor, M. L. Brown, B. D. Fried, H. Grote, J. R. Liberati, G. J. Morales, P, Pribyl, D. Darrow, and M. Ono, Phys. Rev. Lett. **63**, 2365 (1989).

[28]R. R. Weynants and R. J. Taylor, Nucl. Fusion **30**, 945 (1990).

[29]R. R. Weynants, G. Van Oost, G. Bertschinger, J. Boedo, P. Brys, T. Delvigne, K. H. Dippel, F. Durodié, H. Euringer, K. H. Finken, D. S. Fray, J. D. Hey, D. L. Hillis, J. T. Hogan, L. Könen, R. Leners, A. M. Messiaen, A. Pospieszczyck, U. Samm, R. P. Schornm, B. Schweer, G. Telesca, R. Van Nieuwenhove, and P. E. Vandenplas, Nucl. Fusion **32**, 837 (1992).

[30]L. G. Askinazi, V. E. Golant, S. V. Lebedev, V. A. Rozhanskij, and M. Tendler, Nucl. Fusion **32**, 271 (1992).

[31]F. Wagner and U. Stroth, Plasma Phys. Controlled Fusion **34**, 1803 (1992).

[32]W. H. Press, S. Teukolsky, W. T. Vetterling, and B. P. Flannery, *Numerical Recipes in Fortran*, Second Edition, p. 706, (Cambridge University Press, New York, 1992).

[33]S. I. Braginskii, in *Review of Plasma Physics*, edited by M. A. Leontovich (Consultants Bureau, New York, 1965), Vol. 1, p. 205.

[34]A. H. Boozer and G. K. Petravic, Phys. Fluids **24**, 851 (1981).

[35]H. Berk and H. C. Ye, private communication, 1991.

[36]K. T. Tsang, Y. Matsuda, and H. Okuda, Phys. Fluids **18**, 1282 (1975).

[37]F. L. Hinton and R. D. Hazeltine, Rev. Mod. Phys. **48**, 239 (1976).

[38]R. D. Hazeltine and J. D Meiss, *Plasma Confinement*, (Addison-Wesley, 1992).

[39]J. A. Rome and Y-K. M. Peng, Nucl. Fusion **19**, 1193 (1979).

[40]S. I. Krasheninnikov and P. N. Yushmanov, Phys. Plasmas **1**, 1186 (1994).

[41]Y. Z. Zhang, private communication, 1993.

[42]F. L. Hinton and S. K. Wong, Phys. Fluids **28**, 3082 (1985).

[43]A. A. Galeev and R. Z. Sagdeev, Sov. Phys. JETP **26**, 233 (1968).

[44]N. A. Krall and A. W. Trivelpiece, *Principles of Plasma Physics* (San Francisco Press, Inc., 1986).

[45]Wolfram Research, Inc., *Mathematica*™, Version 2.2, (Wolfram Research, Inc., Champaign, 1993).

[46]G.X. Li, R.D. Bengtson, H. Lin, M. Meier, H. Y. W. Tsui, and A. J. Wootton, Nucl. Fusion **34**, 659 (1994).

[47]H. Xiao, R. D. Hazeltine, and P. M. Valanju, Phys. Plasma **1**, 3641 (1994).

FIGURE CAPTIONS

Fig. 1. Sketch of pitch angle scattering.

Fig. 2. Sketch of charge exchange collision.

Fig. 3. Random walk particle diffusion.

Fig. 4. Diffusion coefficient change with collision frequency.

Fig. 5. Sketch of orbit width in toroidal system

Fig. 6. Particle orbit without radial electric field.

Fig. 7. Particle orbit with positive radial electric field.

Fig. 8. Particle orbit with negative radial electric field.

Fig. 9. Average orbit width with different radial electric field.

Fig. 10. Average random walk distance with different radial electric field.

Fig. 11. Ion mobility with pitch angle scattering in banana regime.

Fig. 12. Ion mobility with charge exchange in banana regime.

Fig. 13. Ion mobility with charge exchange in plateau regime.

Fig. 14. Ion diffusion coefficient with charge exchange in plateau regime.

Fig. 15. Ion orbit loss with different radial electric field in banana regime.

Fig. 16. Ion orbit loss with different radial electric field in plateau regime.

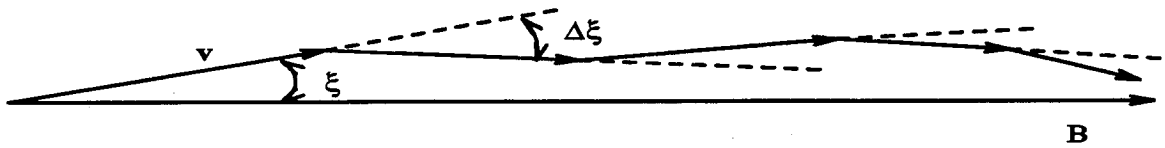

Figure 1: Xiao, PoP–20829

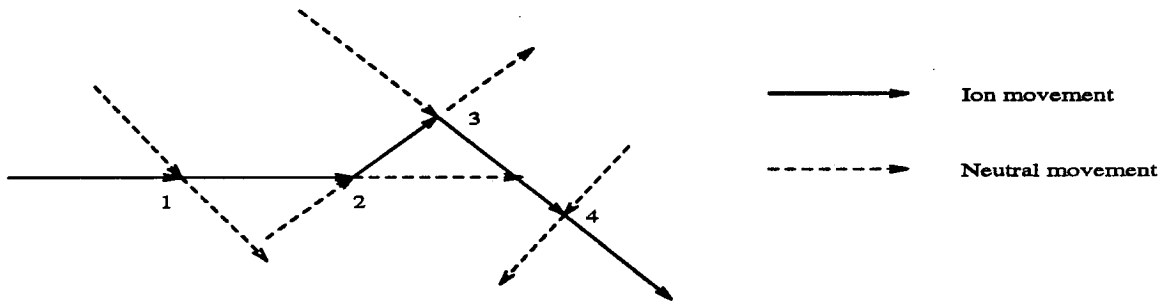

Figure 2: Xiao, PoP–20829

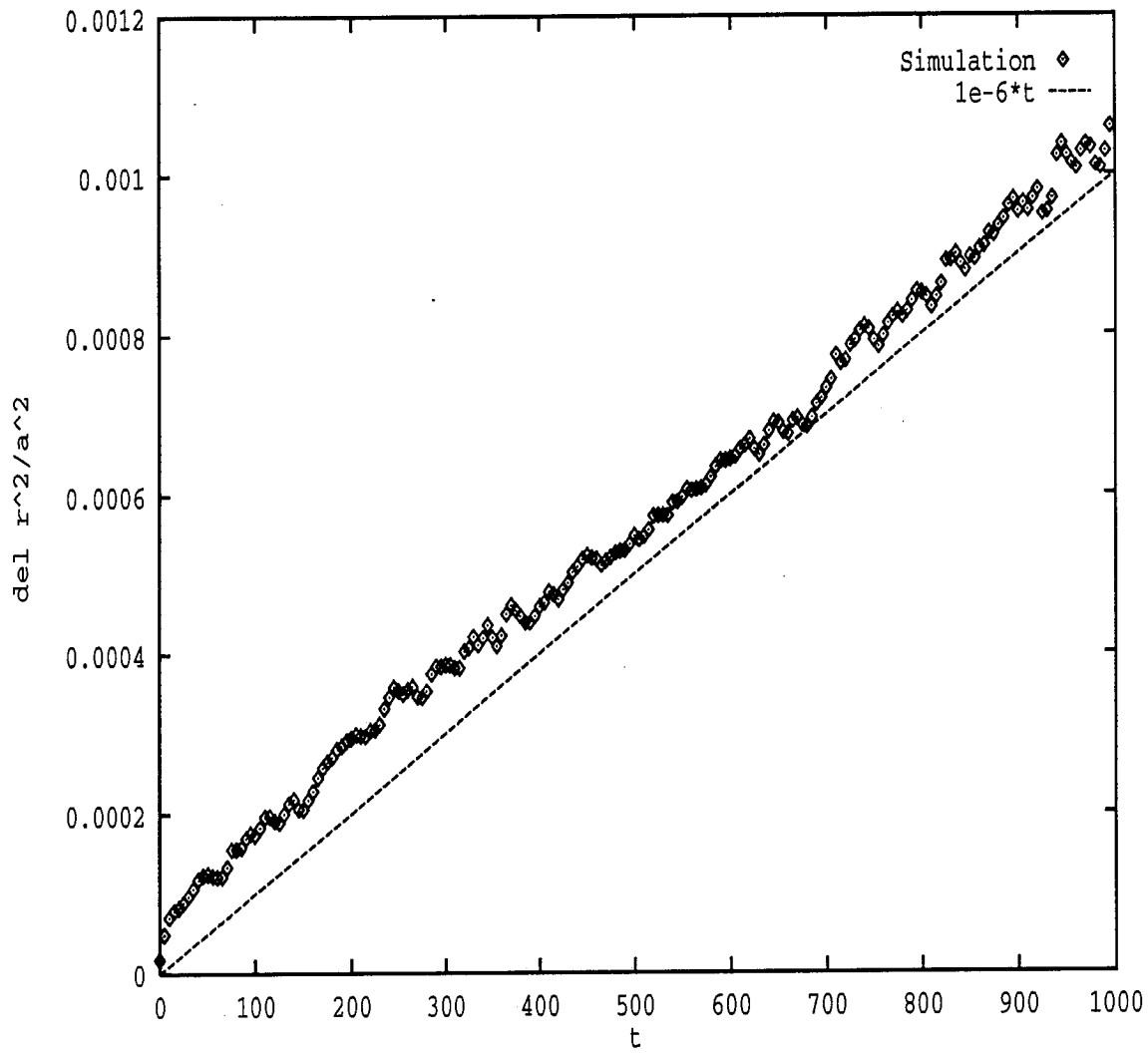

Figure 3: Xiao, PoP–20829

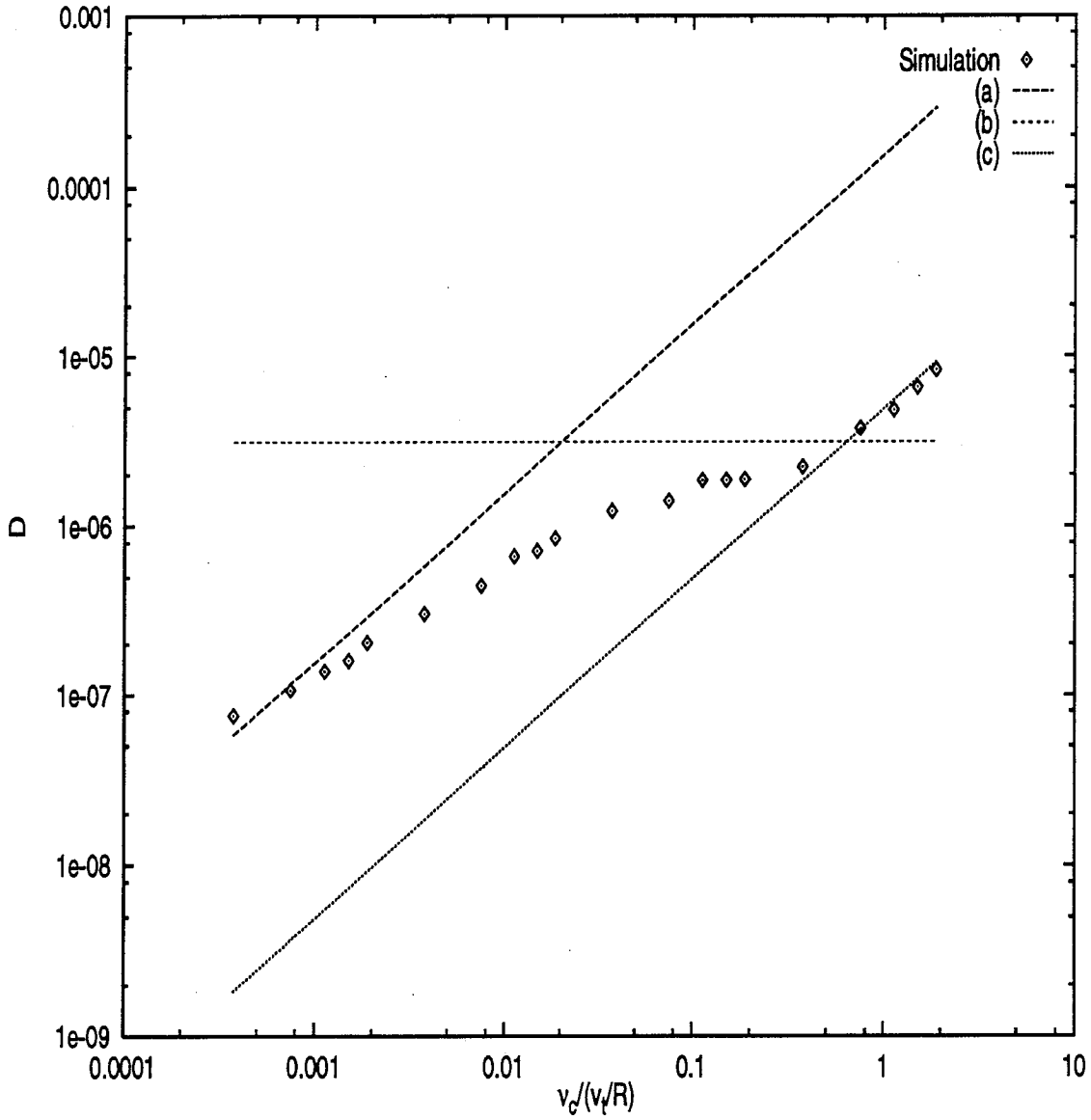

Figure 4: Xiao, PoP–20829

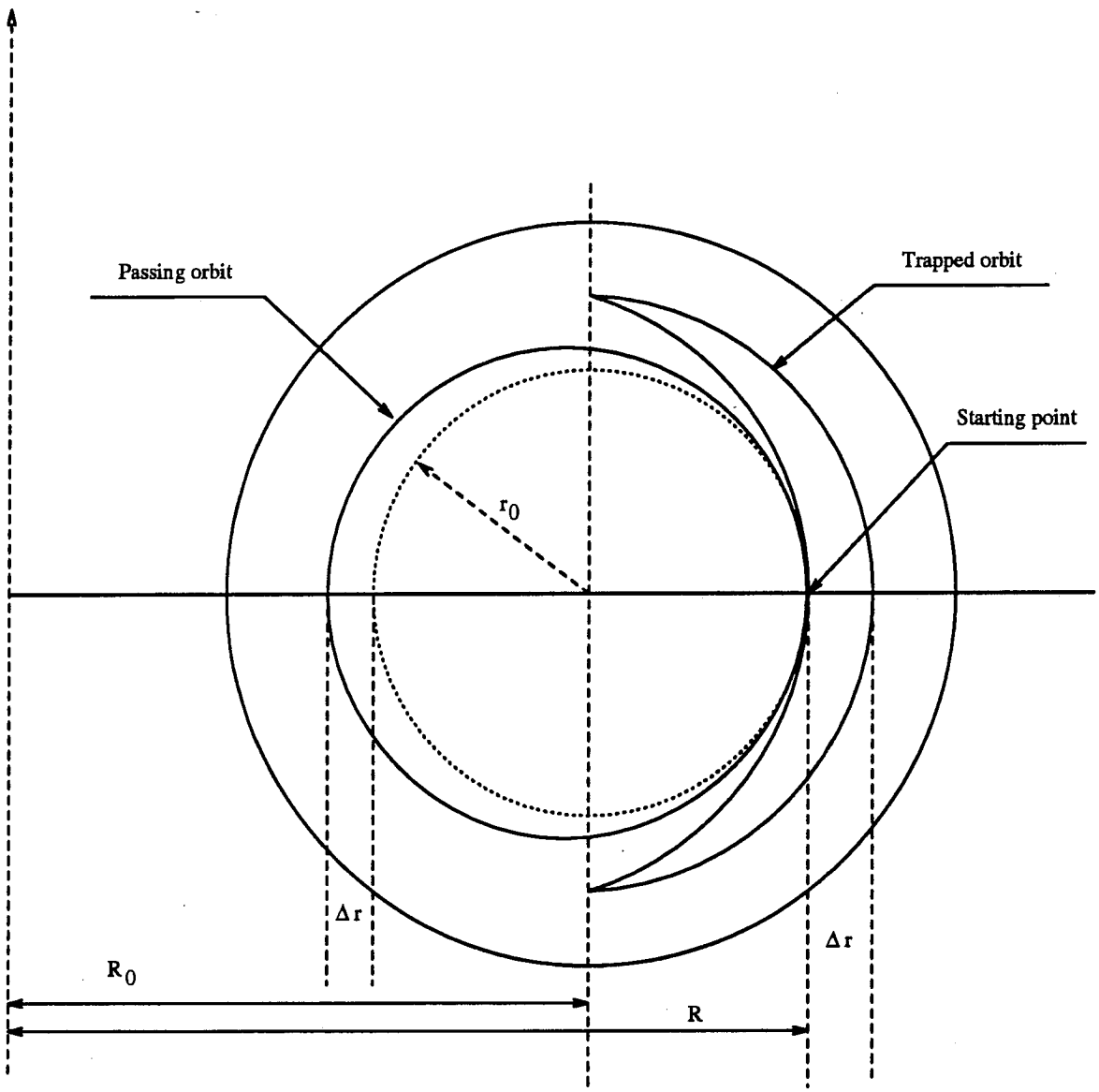

Figure 5: Xiao, PoP–20829

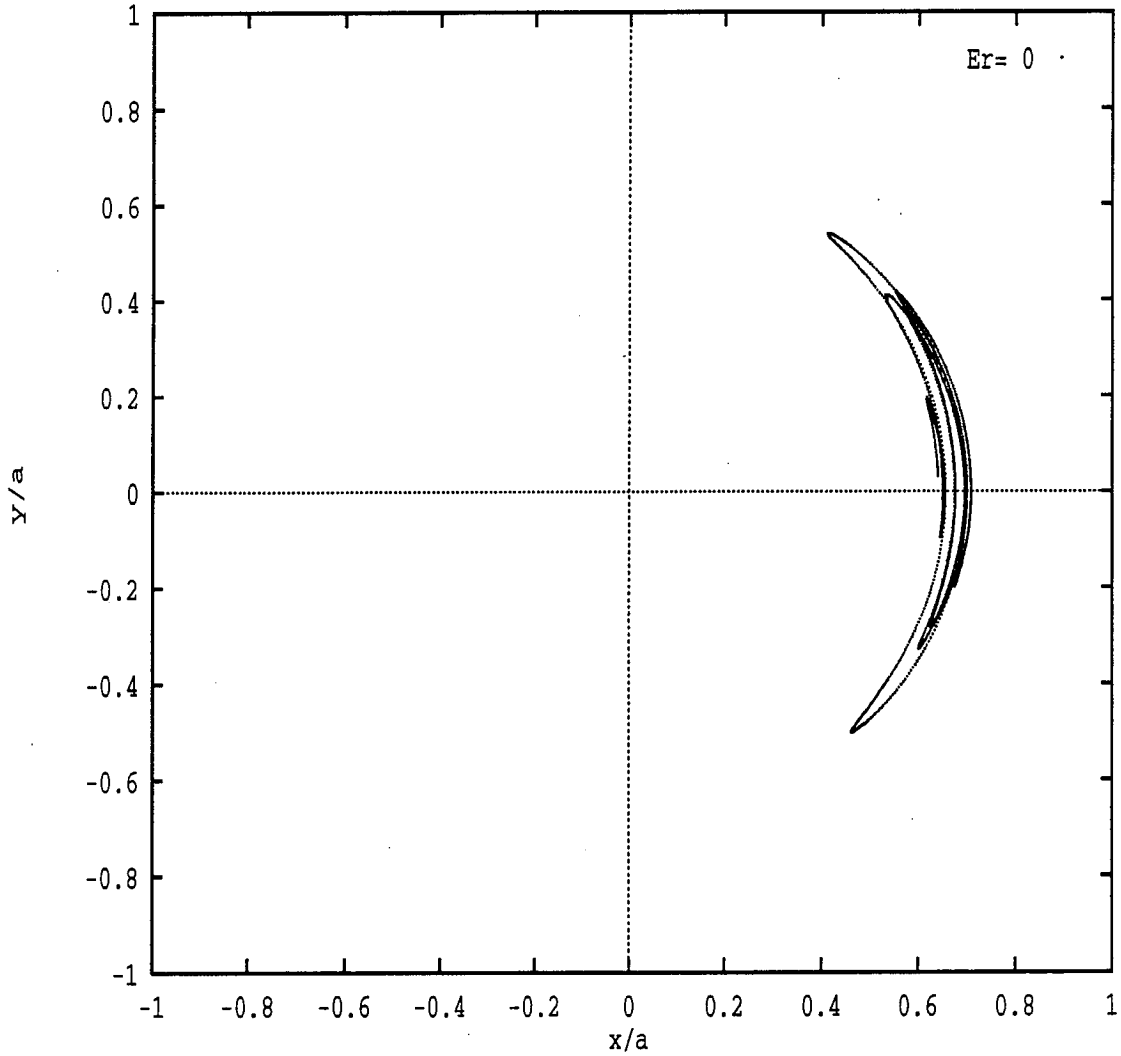

Figure 6: Xiao, PoP–20829

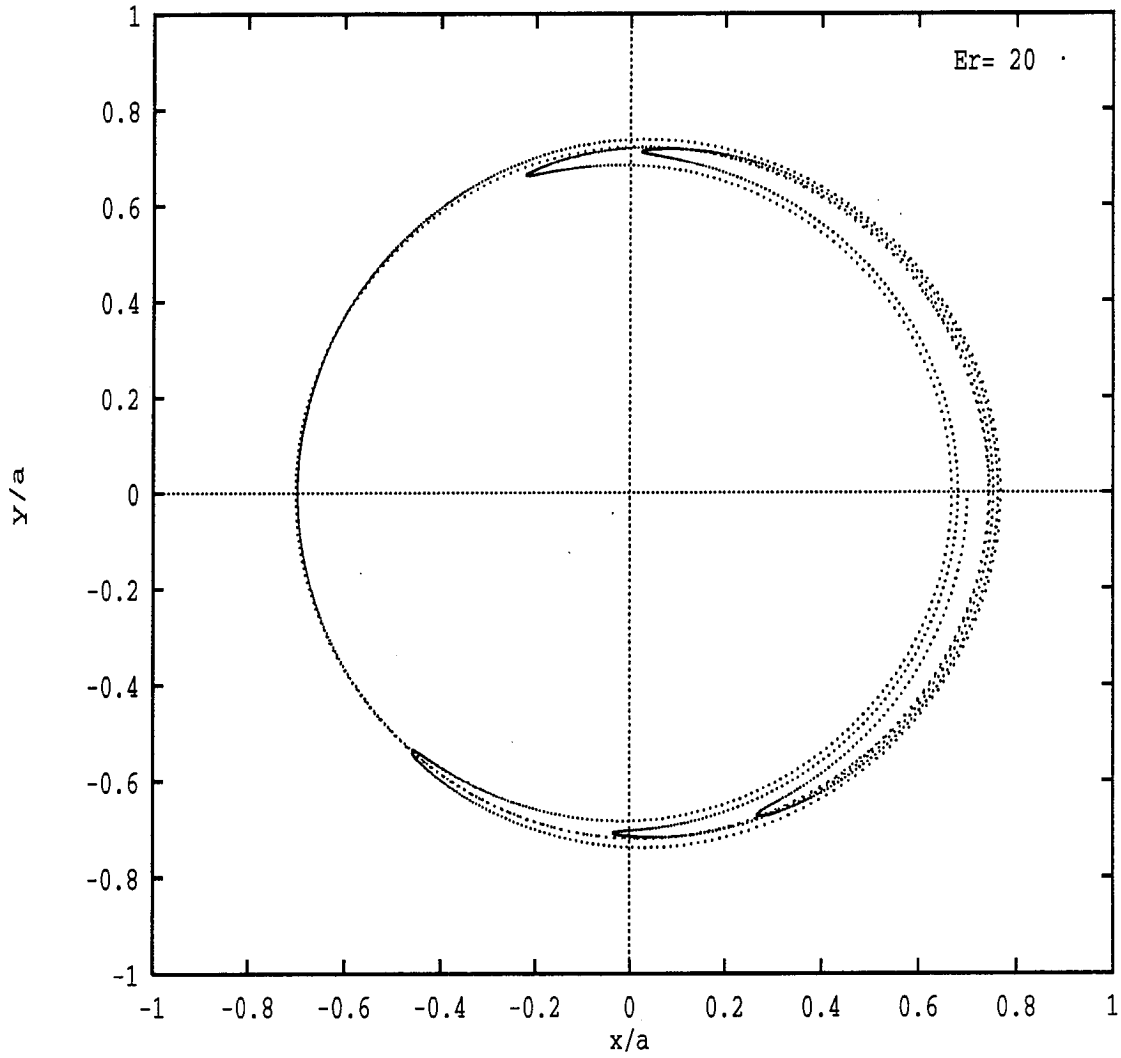

Figure 7: Xiao, PoP–20829

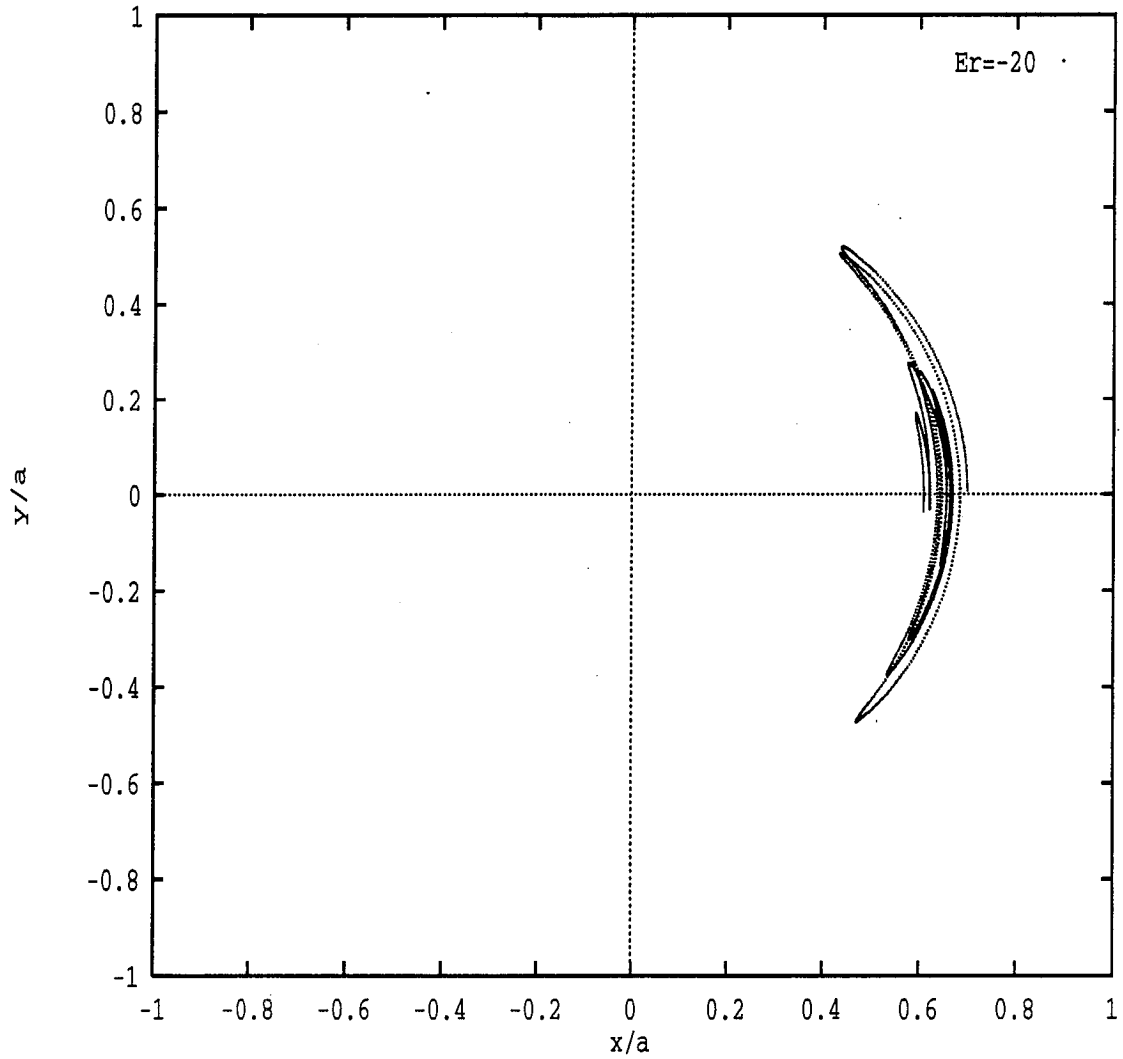

Figure 8: Xiao, PoP–20829

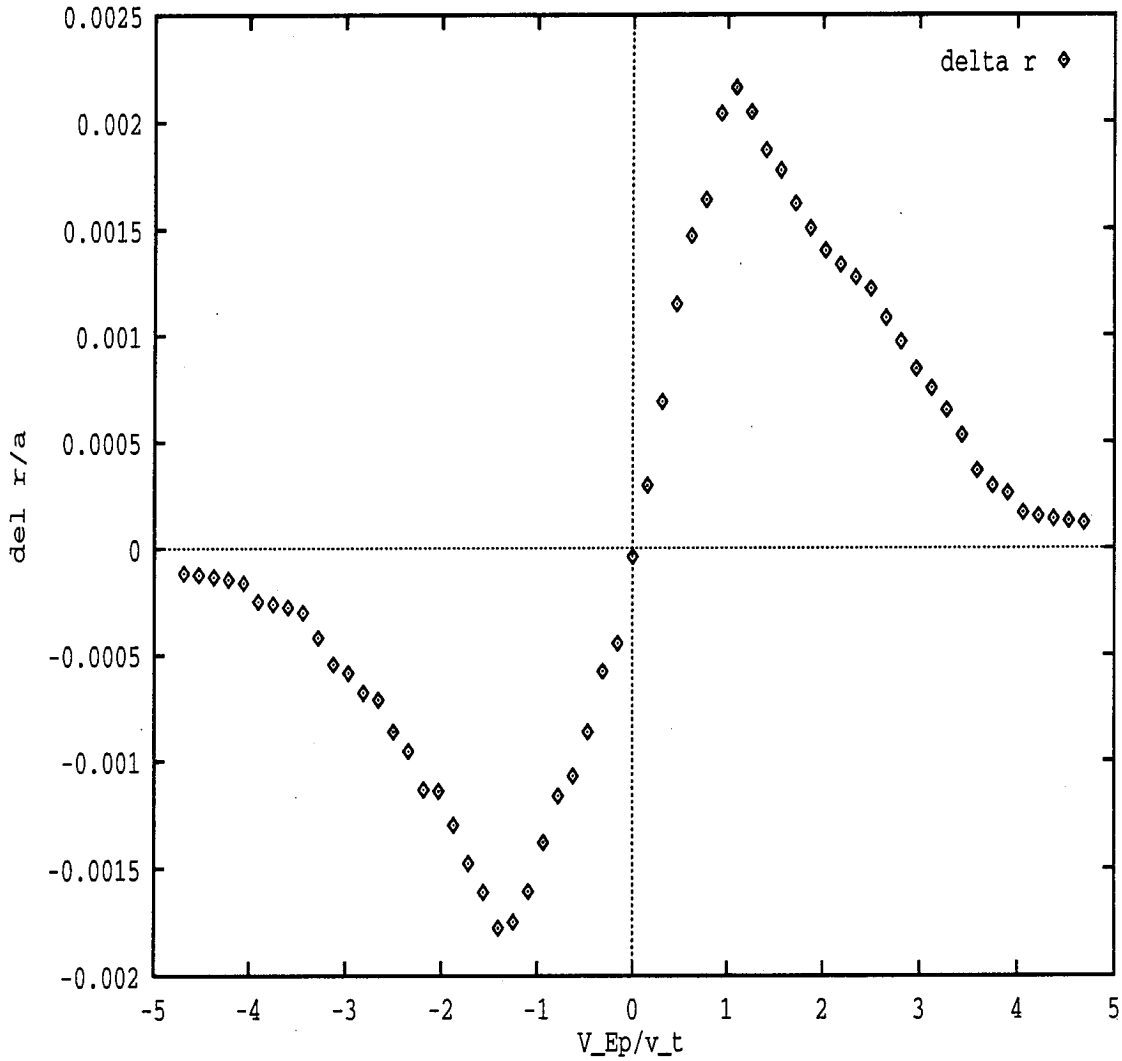

Figure 9: Xiao, PoP–20829

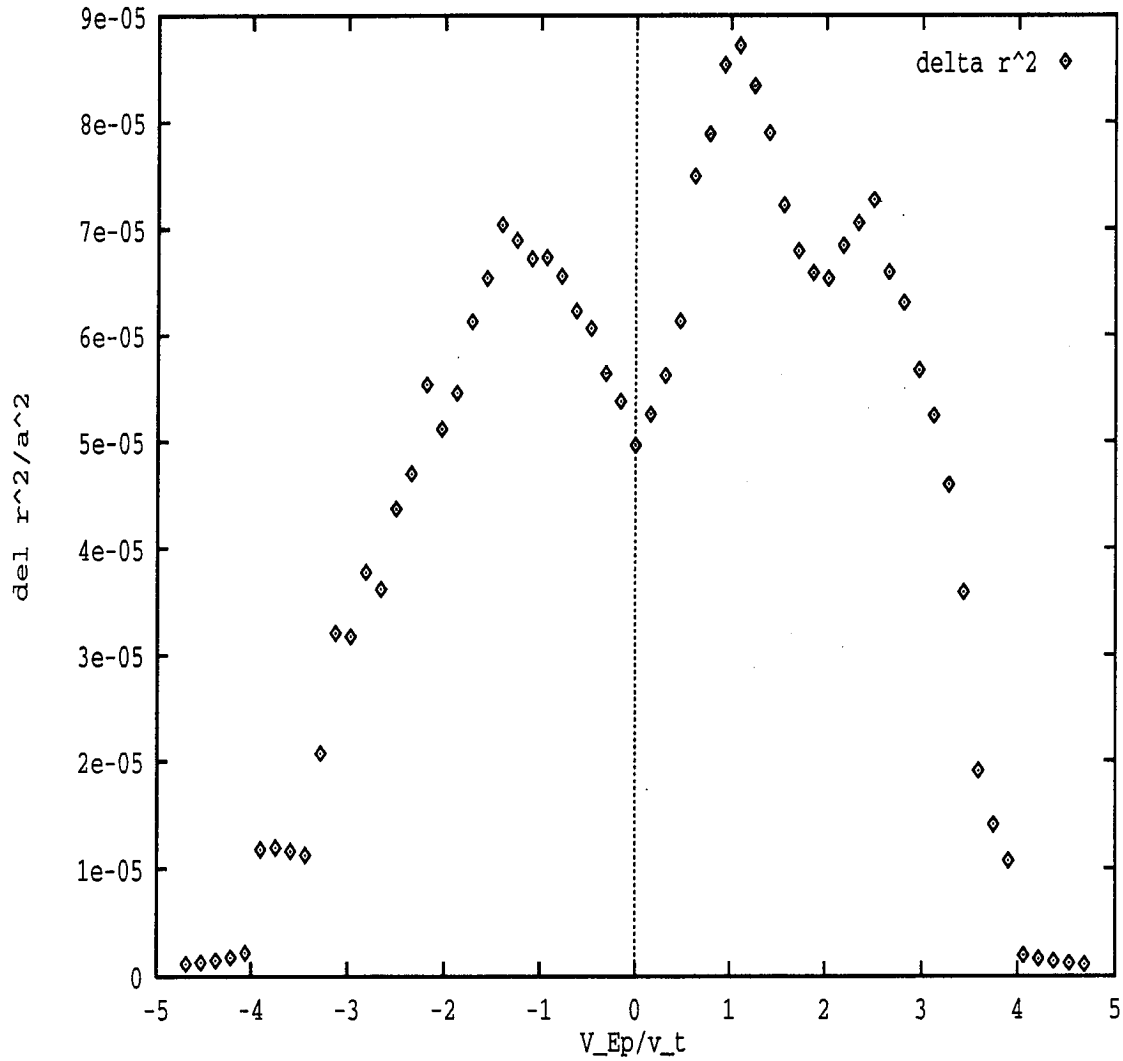

Figure 10: Xiao, PoP–20829

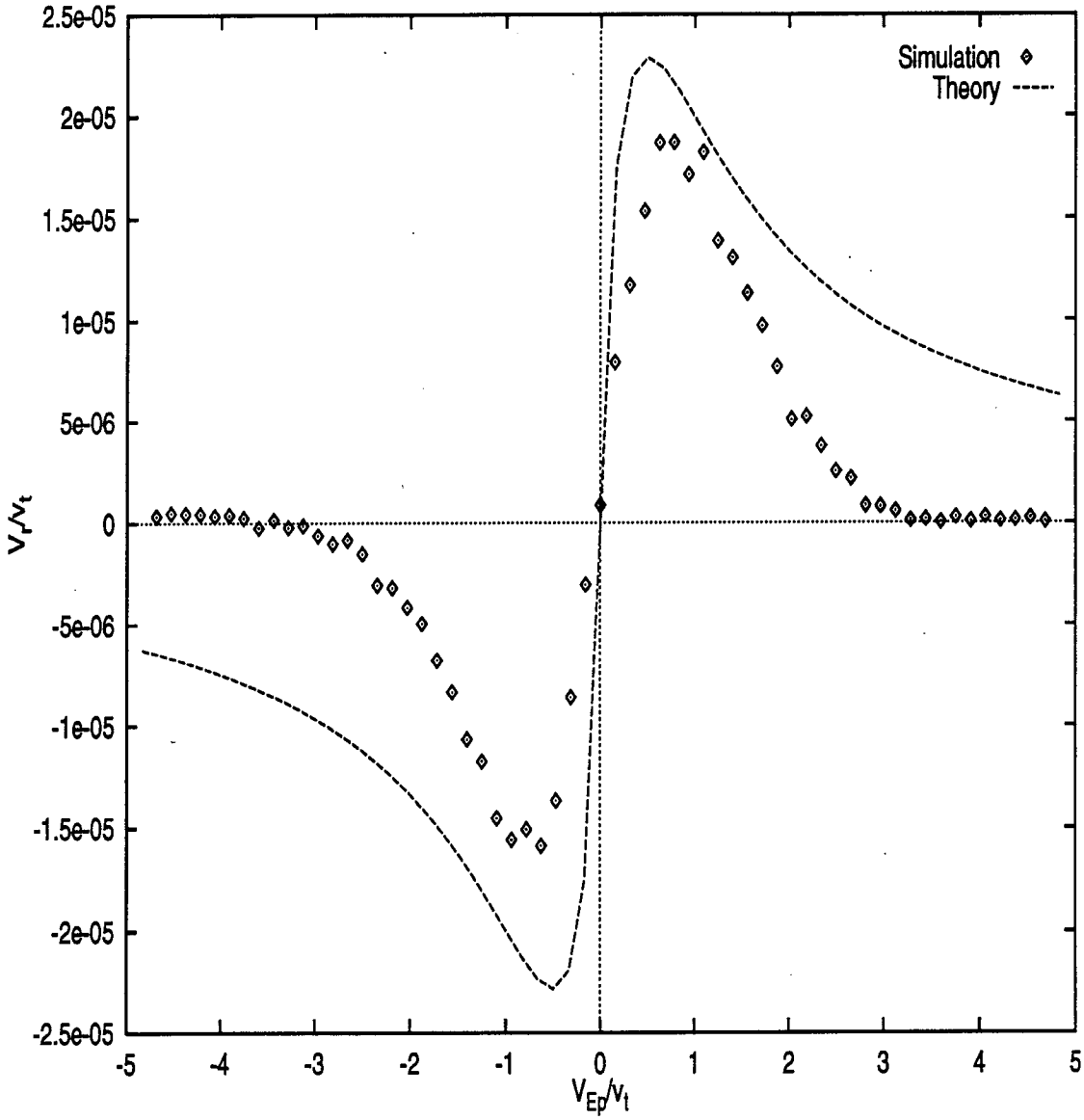

Figure 11: Xiao, PoP–20829

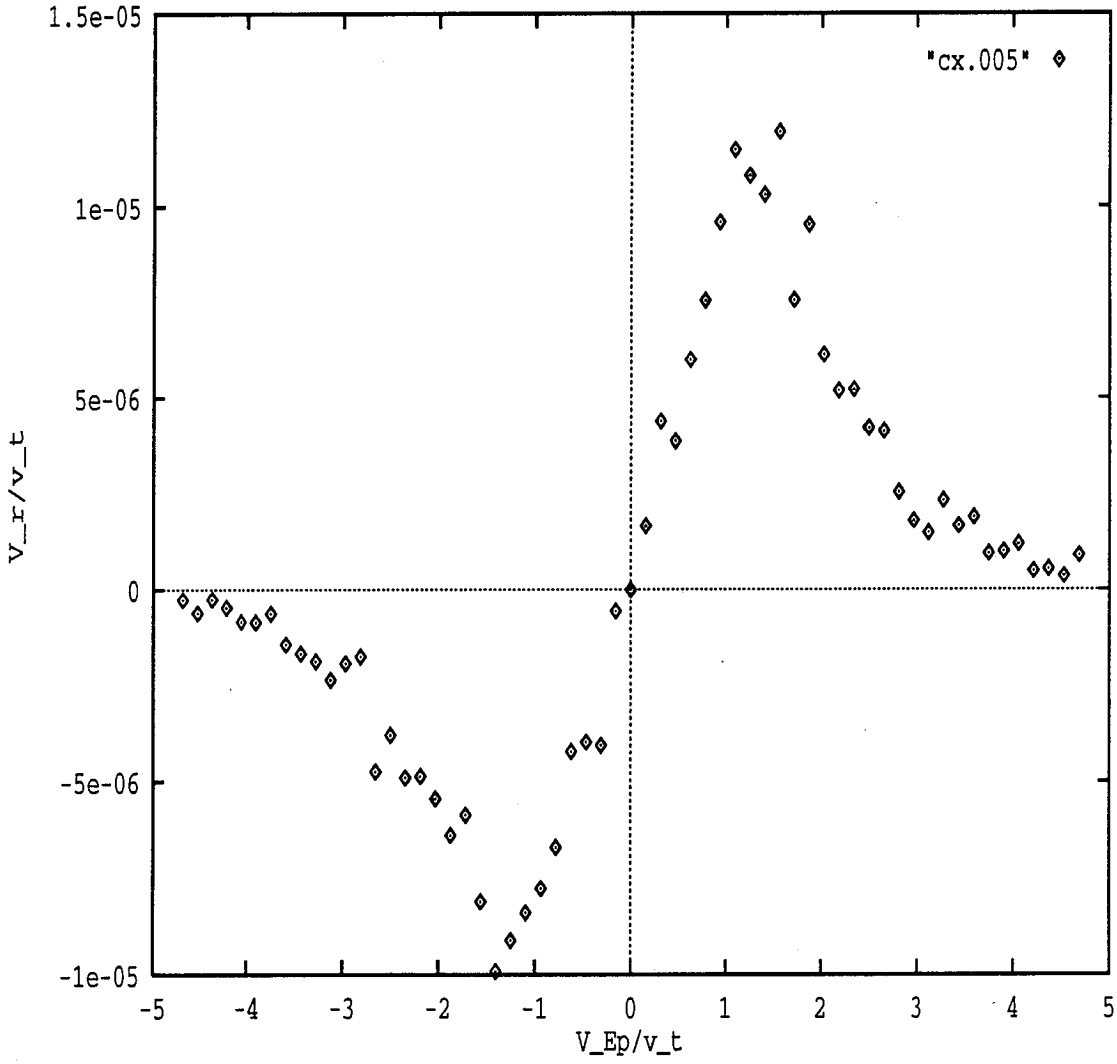

Figure 12: Xiao, PoP–20829

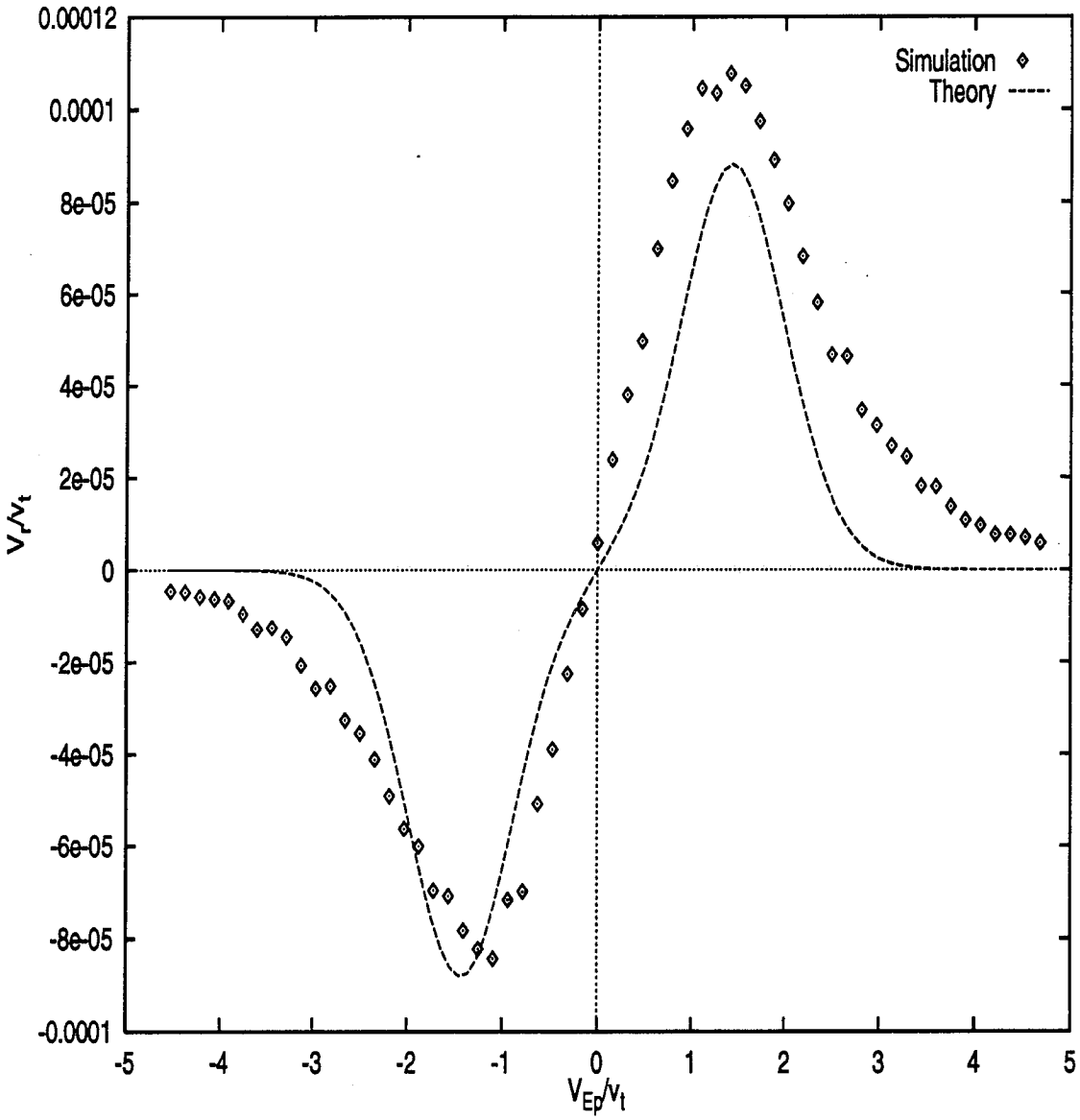

Figure 13: Xiao, PoP–20829

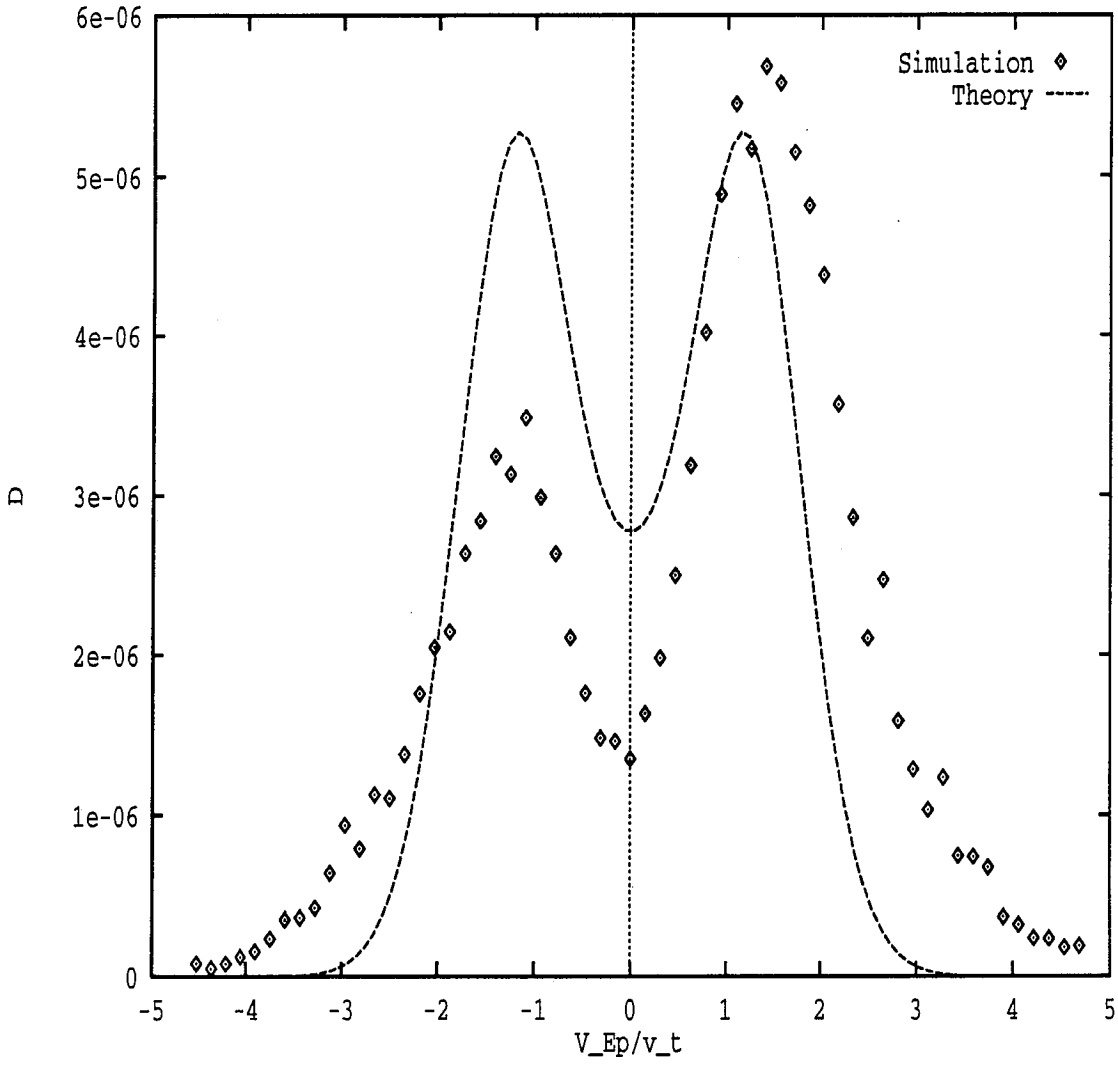

Figure 14: Xiao, PoP–20829

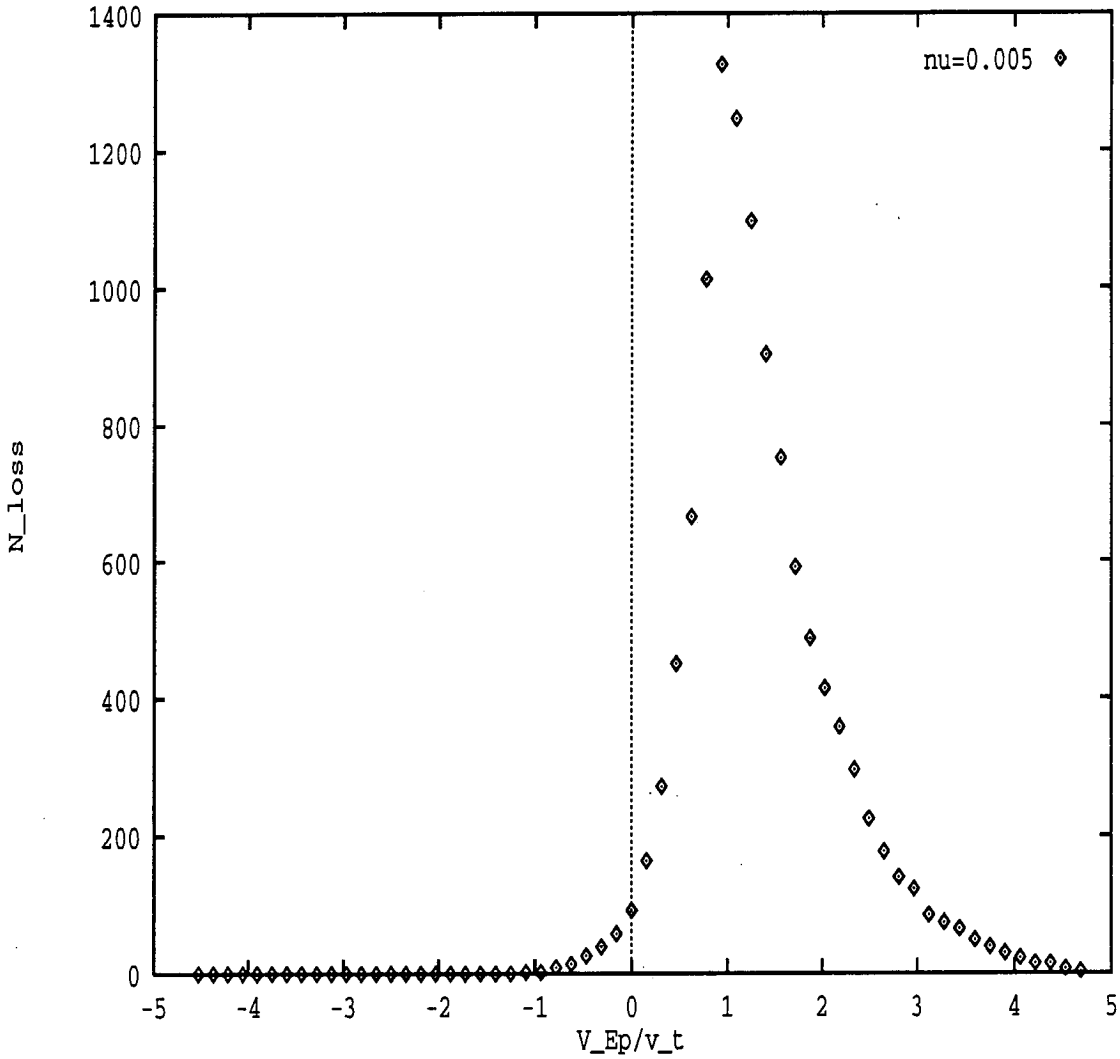

Figure 15: Xiao, PoP–20829

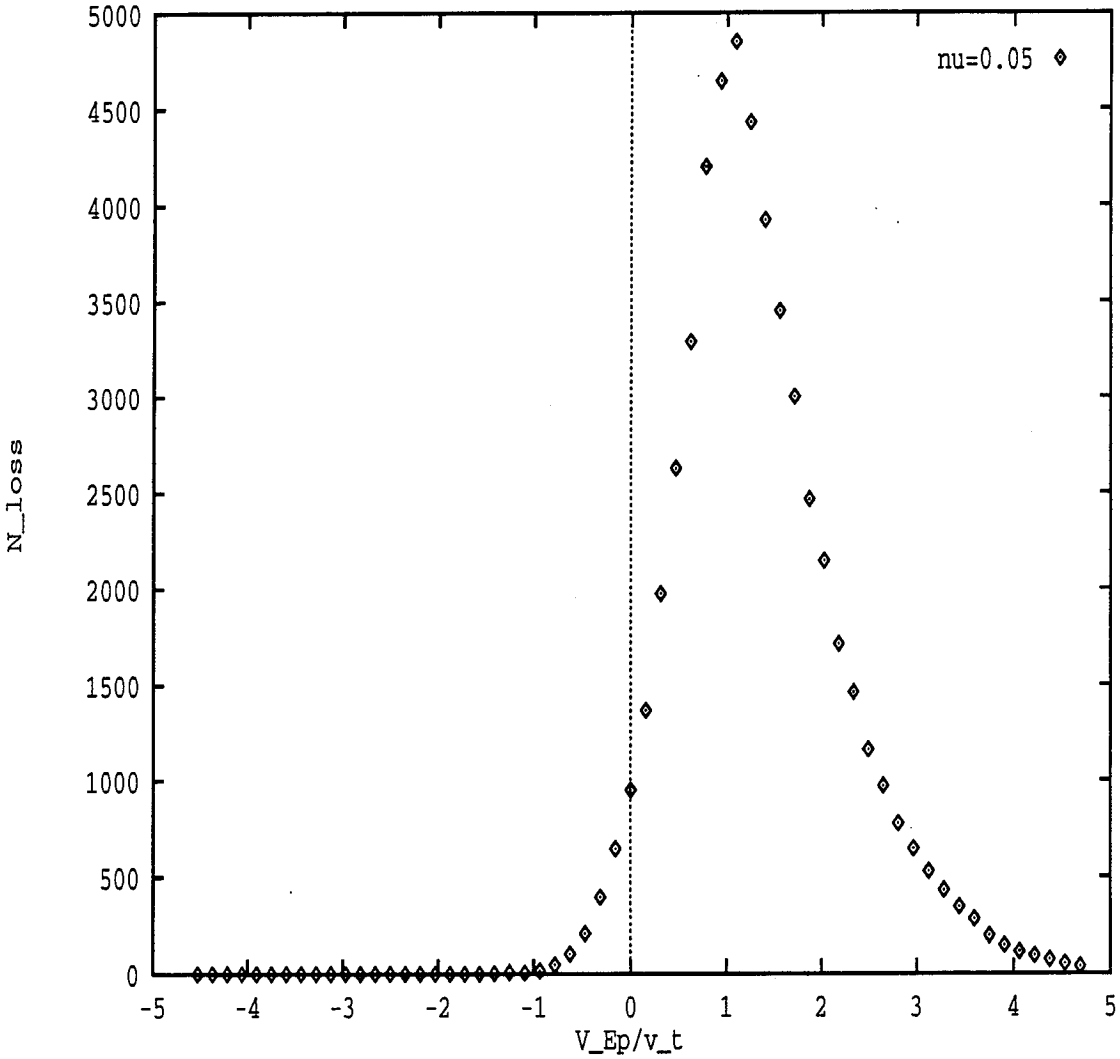

Figure 16: Xiao, PoP–20829